ELSEVIER

Lithos 48 (1999) 263–285

LITHOS

Trace element compositions of minerals in garnet and spinel peridotite xenoliths from the Vitim volcanic field, Transbaikalia, eastern Siberia

Sandra M. Glaser [a], Stephen F. Foley [a,*], Detlef Günther [b]

[a] *Mineralogisch-Petrologisches Institut, Universität Göttingen, Goldschmidtstraße 1, D-37077 Göttingen, Germany*
[b] *Laboratory of Inorganic Chemistry, ETH Zürich, Universitätsstrasse 6, CH-8092 Zürich, Switzerland*

Received 23 April 1998; received in revised form 15 January 1999; accepted 18 January 1999

Abstract

Peridotite xenoliths from the Bereya alkali picrite tuff in the Vitim volcanic province of Transbaikalia consist of garnet lherzolite, garnet–spinel lherzolite and spinel lherzolite varieties. The volcanism is related to the Cenozoic Baikal Rift. All peridotites come from pressures of 20–23 kbar close to the garnet to spinel peridotite transition depth, and the presence of garnet can be attributed to cooling of spinel peridotites, probably during formation of the lithosphere. The peridotites show petrographic and mineral chemical evidence for infiltration by an alkaline silicate melt shortly before their transport to the Earth's surface. The melt infiltration event is indicated petrographically by clinopyroxenes which mimic melt morphologies, and post-dates outer kelyphitic rims on garnets which are attributed to an isochemical heating event within the mantle before transport to the Earth's surface. Single-mineral thermometry gives reasonable temperature estimates of 1050 ± 50°C, whereas two-mineral methods involving clinopyroxene are falsified by secondary components in clinopyroxene introduced during the melt infiltration event. Excimer Laser–ICP-MS analysis has been performed for an extensive palette of both incompatible and compatible trace elements, and manifests the most thorough dataset available for this rock type. Orthopyroxene and garnet show only partial equilibration of trace elements with the infiltrating melt, whereas clinopyroxene and amphibole are close to equilibration with the melt and with each other. The incompatible element composition of the infiltrating melt calculated from the clinopyroxene and amphibole analyses via experimental mineral/melt partition coefficients is similar to the host alkali picrite, and probably represents a low melt fraction from a similar source during rift propagation. The chemistry and chronology of the events recorded in the xenoliths delineates the series of events expected during the influence of an expanding rift region in the upper mantle, namely the progressive erosion of the lithosphere and the episodic upward and outward propagation of melts, resulting in the evolution of the Vitim volcanic field.

Keywords: Peridotite; Xenolith; Melt infiltration; Trace element; Garnet; Spinel; Vitim

1. Introduction

Garnet peridotites form the dominant rock type in cratonic mantle xenolith suites brought to the Earth's surface by kimberlites (Dawson, 1980; Harte, 1983), but are very rare in non-cratonic xenolith suites hosted by alkali basaltic volcanics. This presumably indicates that the generation of alkali basalts and basanites, which are the host lavas to most non-cratonic spinel lherzolite xenolith suites (Menzies,

* Corresponding author

0024-4937/99/$ - see front matter
PII: S0024-4937(99)00032-8

1983) is too shallow to sample garnet peridotites, and that exceptional tectonic circumstances are required to permit sampling in the garnet stability field.

Examples of non-cratonic garnet peridotites which have been described to date appear to occur either in a behind-arc setting entrained in volcanics triggered by asthenospheric upwelling in response to subduction, such as those at Mingxi and Xilong in southeastern China (Cao and Zhu, 1987) and at Pali Aike in southern South America (Skewes and Stern, 1989; Stern et al., 1989), or they occur in rift-related volcanic settings on the flanks of continental rifts, such as the Vitim Plateau in Transbaikalia, eastern Siberia (Ionov et al., 1993) and at the Jetty Peninsula on the flanks of the Lambert–Amery rift in eastern Antarctica (Andronikov, 1990; Andronikov et al., 1998).

Cratonic peridotite xenoliths sampled by kimberlites generally represent very old lithospheric mantle (Pearson, 1998), whereas xenoliths in non-cratonic volcanic provinces represent younger lithospheric mantle domains (Menzies, 1990). Consequently, studies of non-cratonic garnet facies xenoliths hosted in basaltic rocks furnish direct information about the composition of lower levels of the lithospheric mantle away from the cratons and allow us to compare the two xenolith suites and recognise any differences in the development of the lithospheric upper mantle through time.

In this report we present petrographic and mineral chemical details (in situ major and trace element analyses) of newly collected peridotite xenoliths from the Vitim plateau, Eastern Siberia. These peridotites experienced infiltration by melts similar to the host alkali picrites shortly before they were brought to the Earth's surface, and thus represent a case of rift-related metasomatism of garnet peridotites.

2. Geological setting

The Vitim volcanic province is located about 200 km east of Lake Baikal (Fig. 1) close to the Vitim and Dzhilinda rivers. The magmatic activity in this area is associated with the thinning of the lithosphere and the rifting process in the Baikal rift zone, and is summarized by Kiselev (1987). Spinel lherzolite xenoliths have been described from several localities such as Bartoy (Ionov et al., 1992) and the Shavaryn–Tsaram volcano in the Tariat field (Press et al., 1986; Stosch et al., 1986) (Fig. 1), but garnet-bearing peridotites are known only from the Vitim plateau.

Seismic, electrical conductivity and density data indicate that the Baikal rift zone is underlain by anomalous mantle; the seismic velocity at the Moho discontinuity is 0.5 km/s less than under the Siberian platform (Zorin, 1981). It is debated whether the rifting in this region is due to active upwelling of the asthenosphere (Zorin, 1981; Logatchev and Zorin, 1992) or is passive (Kiselev and Popov, 1992). The Baikal Rift was initiated by a change in the intra-plate stress regime of this area as a result of the collision of India and Eurasia in Eocene times, and has developed over the last 30 Ma. The lithosphere beneath the Vitim volcanic field is about 100–125 km thick, and thins rapidly to the northwest, forming the southeasterly flank of the expression of the Baikal Rift in the upper mantle (Fig. 1).

Volcanism in the Vitim plateau area started with the eruption of alkali olivine basalts in the Miocene and continued through the eruption of Quaternary basanites and hawaiites. The samples studied here are from a single occurrence of Miocene alkali picritic tuffs at the Bereya quarry, which is the locality referred to by Ionov et al. (1993) as the ''tuff pit''. The Bereya quarry is located towards the eastern edge of the Vitim province, and a K/Ar age of 16.3 Ma is reported by Esin et al. (1995) for the host alkali picrite tuff. Due to the abundance of garnet peridotites the Bereya quarry is unique even within the Vitim area: garnet or garnet–spinel bearing varieties make up about 80% of the lherzolite xenoliths.

3. Petrography and mineral chemistry

Most of the xenoliths were collected from the Romanovka–Bagdarino road and others directly from the Bereya quarry from which the road material was excavated. Ionov et al. (1993) remarked that the Vitim peridotites show little evidence for metasomatic enrichment, although they focused their atten-

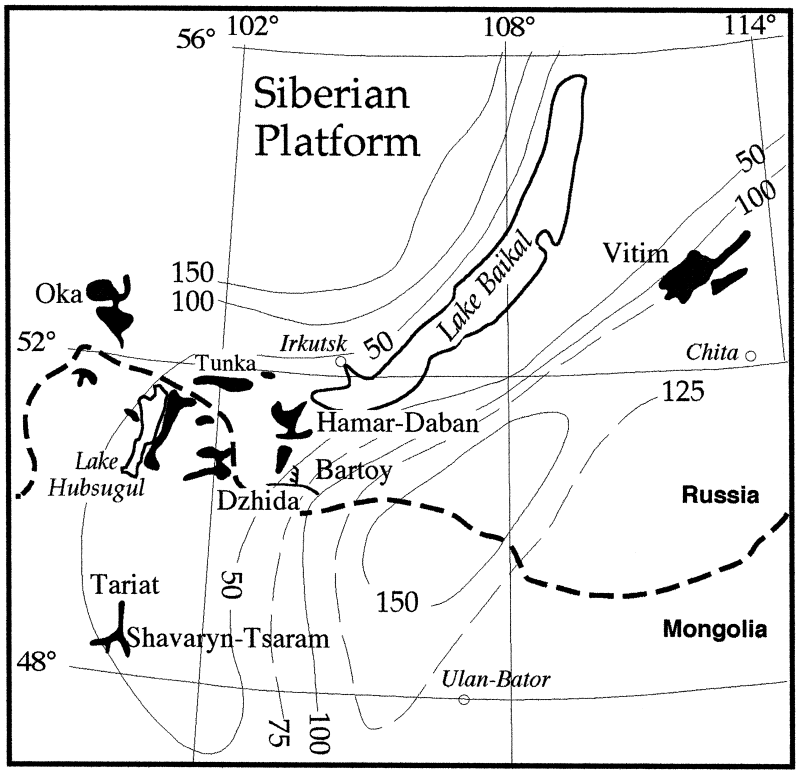

Fig. 1. Geological setting of the Vitim volcanic province showing positions of volcanic fields (black areas) associated with the Baikal Rift and contours of depths to the base of the lithosphere as defined by Zorin et al. (1989). Large towns are shown in italics. The Bereya alkali-picrite garnet peridotite xenolith locality lies at the eastern edge of the Vitim volcanic field (''tuff pit'' locality in Ionov et al., 1993).

tion on rare large samples (up to 30 cm) in a study aimed at comparing the least metasomatised garnet peridotites from cratonic and non-cratonic regions. We have investigated the more common smaller samples, which have an average size of 5–6 cm, and can be subdivided into several groups: (1) garnet lherzolites, (2) garnet–spinel lherzolites, (3) spinel lherzolites, and (4) pyroxenites. Amphibole- and phlogopite-bearing examples of all groups except the garnet peridotites are represented in our collection. We have concentrated on the lherzolite xenoliths; information on the variable and extensive pyroxenite suite and on other xenolith types such as megacrysts and granulites is given elsewhere (Ashchepkov et al., 1994; André and Ashchepkov, 1996; Litasov and Litasov, 1999). Seven xenoliths were selected as representatives of the peridotite groups for in situ trace element analysis by Laser–ICP-MS. The following description of petrographic and mineral chemical features is based on these selected samples but is representative of the suite as a whole.

3.1. Petrographic features of the Bereya peridotites

The xenoliths of the peridotite groups consist of variable amounts of olivine, orthopyroxene and clinopyroxene (4–21 vol.% with the exception of one harzburgite sample, determined by point counting; Fig. 2, Table 1). This confirms the observation of Ionov et al. (1993) that the peridotites vary between depleted and fertile compositions, whereby fertile compositions are much commoner than in most mantle regions, including garnet lherzolites from cratonic regions (Boyd, 1989; Boyd et al., 1997; Rudnick et al., 1994) and spinel lherzolites from non-cratonic regions (Frey and Prinz, 1978; Bernstein et al., 1998). Minor phases include garnet

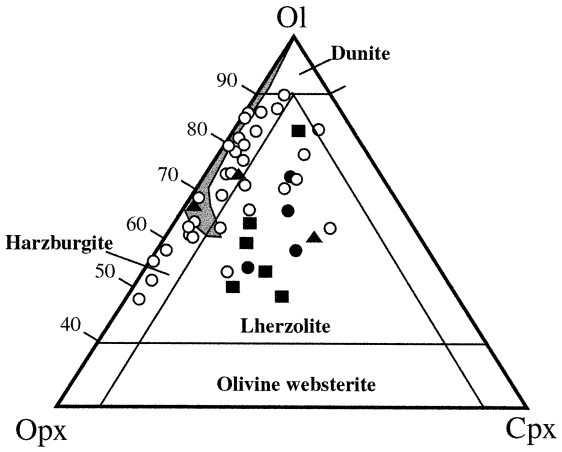

Fig. 2. Modal mineralogy of xenoliths from Bereya compared to Kaapvaal garnet lherzolites (open circles; Nixon, 1987) and depleted spinel lherzolites from Wiedemann, West Greenland (shaded field; Bernstein et al., 1998) showing the higher abundance of clinopyroxene in the Bereya samples (filled symbols: circles = garnet peridotites, squares = garnet spinel peridotites, triangles = spinel peridotites).

Table 1
Mineral modes in Bereya peridotites
Modes are given in vol.% as determined by point counting in thin section. Trace element analyses are available for samples marked with an asterisk.

Sample	Ol	Opx	Cpx	Gt	Sp	Amph	Phl
SF-93102	56.6	24.7	16.0	2.1	0.7		
SF-93193	53.2	30.3	13.1	1.7	0.7		
SF-93200	63.6	22.0	9.6	2.0	0.8		
SF-93207	55.7	22.5	10.0	11.8	< 0.35		
SG-96B14	52.2	24.6	20.6	2.6	0.7		
SF-93112	75.2	19.7	4.1		0.9		
SF-93118	63.1	14.7	19.7		1.1		
SG-96B11*	68.7	28.2	0.5		1.3	0.8	0.5
SF-93163*	63.5	15.4	13.3	6.6	< 0.4		
SF-93205*	71.1	12.4	11.2	5.4			
SF-93182	55.2	17.3	16.9	8.9	< 0.4		1.3
SG-96B13*	57.1	26.7	13.6	1.9	0.3		0.5

(2–12 vol.%) and/or spinel (0.3–1.3 vol.%), and many rocks contain rare phlogopite and/or amphibole (generally less than 1 vol.%). However, our suite does not contain the amphibole–phlogopite veins described by Ionov et al. (1993), presumably due to the smaller size of the samples.

We retain the nomenclature of Ionov et al. (1993) in reserving the term garnet peridotite for rocks which contain only spinel as inclusions in garnet, whereas garnet–spinel peridotites also contain larger spinel grains outside garnet. Ionov et al. (1993) showed by reference to a composite xenolith that this distinction may be due largely to differences in bulk composition and not to depth of origin. Textural relations are compatible with the formation of garnet by the reaction

spinel + clinopyroxene + orthopyroxene
→ garnet + olivine

which is often documented by inclusions of the reactant minerals within garnet, and the restriction of spinel to inclusions within garnet in the garnet peridotites. Early and late stages of the reaction have also been found in Bereya samples.

Fig. 3. Photomicrographs of the Bereya lherzolite xenoliths. (a) Typical texture of lherzolites showing elongate grains with equilibrium 120° triple junctions. Photo width = 4.5 mm. (b) Sheared spinel lherzolite with porphyroclasts of olivine, orthopyroxene and clinopyroxene in mosaic matrix of the same minerals which lacks the strong preferred orientation typical of sheared xenoliths in kimberlites. Photo width = 4.5 mm. (c) Phlogopite-bearing lherzolite contrasting the textures of the two clinopyroxene generations. The first (Cpx-1) forms approximately equant grains 0.2–2 mm across and is interpreted as an integral part of the lherzolite prior to melt infiltration. Grain boundaries are often concave against olivine and orthopyroxene. The second generation (Cpx-2) forms optically continuous crystals filling interstitial passageways between several crystals of the original lherzolite. A late recrystallised rim (10–100 μm wide) occurs on both generations. Photo width = 4.5 mm. (d) Infiltration and breakdown textures in garnet lherzolite. Garnet (Gt) grains and subgrains are reacted to form a thin brown kelphitic rim (Kp). Second generation Cpx (Cpx-2) forms interstitial networks around other minerals and has thin recrystallised rims (cr) interpreted as being formed by decompression breakdown during ascent to the Earth's surface. Photo width = 4.5 mm. (e) Clinopyroxene interstitially occupying a triple junction between olivine and opx forming apparent dihedral angles much too small for textural equilibrium between these minerals. Circular structures are ablation pits from LAM–ICP-MS analysis of 40–80 μm diameter. Photo width = 0.55 mm. (f) Larger area including the area of (e) (upper left) showing that cpx surrounds earlier minerals and replaces melt morphology. Photo width = 1.1 mm.

The textures of the peridotites are similar to the typical protogranular type of spinel peridotites from alkali basalts (Mercier and Nicolas, 1975), with garnet forming irregular grain shapes. Crystals generally have straight or gently curved boundaries and show only little evidence of strain in the form of undulose extinction. Typical grain sizes for olivine and orthopyroxene are 2–4 mm, for spinel approximately 0.2 mm, whereas garnet ranges in size from 0.5 up to 6.5 mm. Olivine often forms elongated prismatic grains resulting in a weak preferred orientation, although even here triple-grain junctions approach 120°

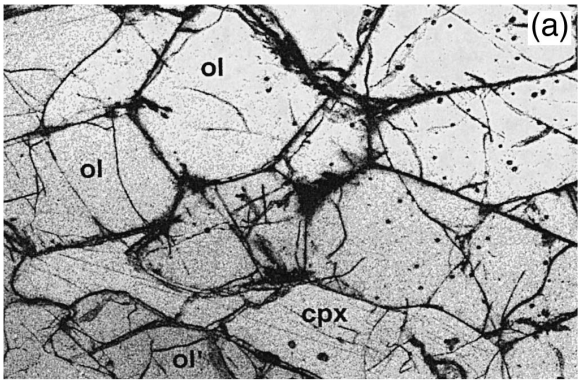

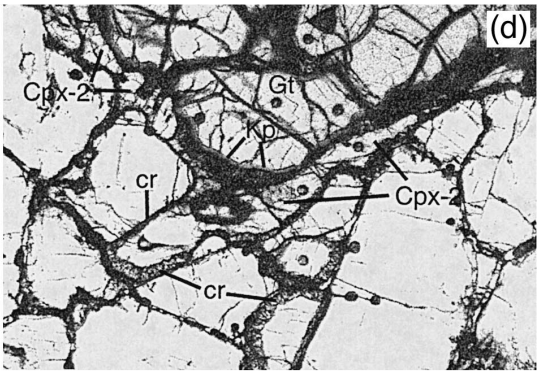

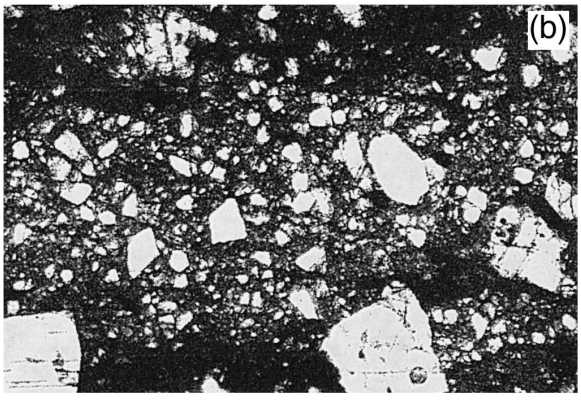

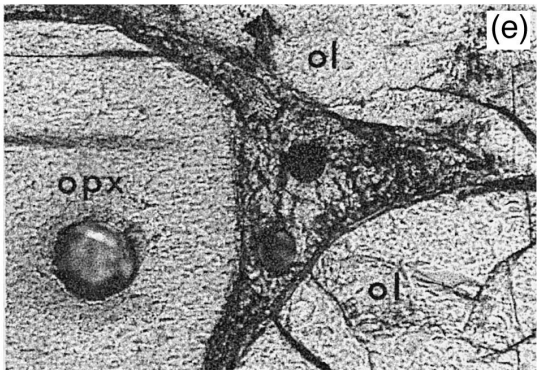

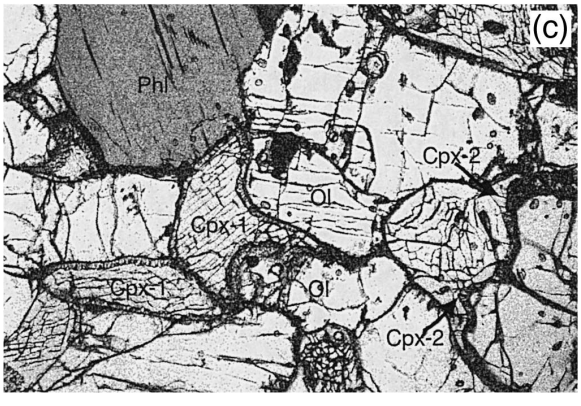

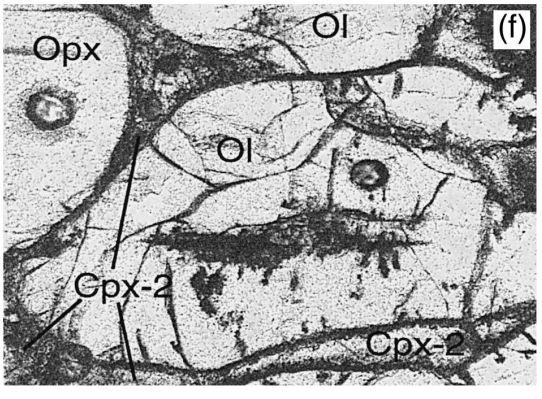

angles (Fig. 3a). An exception is sample SF-93162 which shows a strongly deformed porphyroclastic mosaic texture consisting of a fine-grained matrix of recrystallized olivine, orthopyroxene and clinopyroxene surrounding porphyroclasts of the same phases (Fig. 3b). This xenolith contains veins of glass probably resulting from contact with the ascending magma.

Amphibole appears only in spinel–harzburgite sample SG-96B11 and in the pyroxenite SF-93803. In sample SF-93803 amphibole forms a vein through the xenolith and is surrounded by a thin mosaic rim of orthopyroxene and olivine, whereas in sample SG-96B11 it appears as well-rounded inclusions (up to 200 μm) in all lherzolite mineral phases. Phlogopite-bearing examples of both garnet–spinel (SG-96B13) and spinel lherzolites (SG-96B11) have been studied. Phlogopite occurs as large (2–3 mm) subequant to elongate strongly pleochroic crystals (Fig. 3c) often with glass on grain boundaries, particularly in contact with orthopyroxene.

Clinopyroxene occurs as two texturally distinguishable generations. The first consists of approximately equant grains 0.2–2 mm across (Cpx-1 in Fig. 3c), many of which appear xenomorphic due to grain boundaries which are concave towards the clinopyroxene (Fig. 3c, centre). The second generation consists mostly of long irregular crystals which form optically continuous interstitial networks between several other mineral grains; these may be continuous over 2 cm in section or surround several surfaces of olivine or garnet crystals (Cpx-2 in Fig. 3c,d,f). Clinopyroxenes of both generations usually have thin reacted rims consisting of recrystallised clinopyroxene and glass (Fig. 3c and d); these occur irrespective of the identity of the neighbouring grain, and were probably produced within the host magma during transport to the Earth's surface.

Garnets exhibit two types of reaction corona, a ubiquitous, microscopically amorphous brown rim (Kp-1; Fig. 3d) reminiscent of kelyphites in garnet lherzolites and garnet megacrysts in kimberlites, and a very fine-grained intergrowth of clinopyroxene, orthopyroxene and greenish spinel (Kp-2) forming a reaction zone generally not more than 50 μm wide. The first type is present also on subgrain boundaries, whereas the second occurs discontinuously on outer rims of garnets in contact with other silicate phases. The reaction forming Kp-2 is the reverse of the garnet-building reaction and may be isochemical, in contrast to the kelyphite-forming reaction in many peridotites entrained in kimberlites, which appear to require the introduction of a metasomatic component (Hunter and Taylor, 1982). Kp-2 occurs outside Kp-1 and rarely between Kp-1 and the recrystallised rims of clinopyroxenes (cr in Fig. 3d).

Some textural features of the second generation clinopyroxenes may be explained by the infiltration of melt into the peridotites within the mantle. The irregular shapes of Cpx-2 with extreme aspect ratios (Fig. 3c,d,f) and very low contact angles ($< 40°$) between Cpx-2 and olivine and/or orthopyroxene (Fig. 3e) indicate the crystallisation of Cpx-2 in space previously occupied by a melt: the morphology of Cpx-2 and the low apparent dihedral angles resemble those of melt pockets in partially molten ultramafic rocks (Faul, 1997; Cmíral et al., 1998). Dihedral angles such as in Fig. 3e are far too small to represent equilibrium contact angles between silicate minerals; measurements on a similar occurrence in the Inagli dunite of eastern Siberia show some of these contact angles to be close to those expected for olivine/melt and orthopyroxene/melt (Zinngrebe et al., 1995), whereas others are intermediate between the angles expected for melt and for clinopyroxene, indicating various degrees of subsolidus textural re-equilibration.

3.2. Mineral chemistry

Major element compositions of minerals were analysed by Cameca SX 51 electron microprobe at the University of Heidelberg. Mineral compositions correspond broadly to the observations of Ionov et al. (1993): major element analyses are given in Tables 2–7 only for minerals which were also analysed for trace elements, whereas the following brief summary is based on a larger sample set.

Olivines in the Bereya peridotites are unzoned with forsterite contents from 89 to 91. The Mg# ($100\ Mg/(Mg + Fe)$) is slightly higher in spinel peridotites than in garnet peridotites. On a plot of modal olivine content against Mg# of olivines (Fig. 4), Bereya peridotites plot clearly in the region typical for fertile non-cratonic spinel lherzolites (Boyd,

Table 2
Major and trace element compositions of olivines
Major elements by electron microprobe, trace elements by LAM–ICP-MS in Tables 2–7; n = number of analyses averaged for the LAM–ICP-MS data.

wt.%	Gt-peridotites		Gt–Sp-peridotites		Sp-peridotites		Pyroxenite
	SF-93163	SF-93205	SG-96B13	SF-93174	SG-96B11	SF-93162	SF-93803
SiO_2	41.01	40.50	40.94	40.97	40.99	40.91	39.99
TiO_2	0.01		0.01	0.01			0.05
Al_2O_3	0.04	0.01	0.02	0.06	0.05		0.03
MgO	49.10	48.29	49.17	49.43	48.93	49.41	45.76
FeO	10.13	9.84	9.43	9.82	10.26	10.01	12.77
CaO	0.10	0.05	0.07	0.09	0.06	0.03	0.05
Na_2O	0.03		0.02	0.02	0.02		
K_2O	0.01		0.01			0.02	
Total	100.78	99.12	100.10	100.95	100.46	100.88	99.17
n	7	4	4	2	7	3	3
ppm							
Cs							
Rb	< 0.03		< 0.05	< 0.04	< 0.06		
Ba	< 0.09		< 0.08	< 0.11	0.04		
Th	< 0.003	0.010	0.003	< 0.003	0.005	< 0.003	< 0.003
U	< 0.003	0.008	< 0.01	< 0.003	< 0.003	< 0.01	0.006
Nb	0.028	< 0.07	< 0.05	0.008	< 0.05	< 0.10	< 0.11
Ta	0.003	< 0.02	< 0.01	< 0.003	< 0.01	< 0.02	0.005
La	0.017	0.015	0.007	0.003	< 0.02	< 0.02	0.009
Ce	0.047	0.099	0.028	0.008	0.067	0.06	< 0.02
Pr	0.005	< 0.01	< 0.01	< 0.003	< 0.01	< 0.02	< 0.03
Sr	0.32	0.12	0.025	0.072	0.18	0.17	0.18
Nd	0.017	0.032	< 0.02	< 0.003	< 0.05	< 0.05	< 0.09
Sm	0.007	0.035	< 0.05		< 0.14	< 0.16	< 0.23
Zr	0.090	0.073	< 0.08	0.056	0.20	0.007	0.15
Hf	0.003	0.014	0.007	< 0.003	0.004	< 0.06	< 0.06
Eu	0.004	0.013	< 0.01	< 0.003	0.007	< 0.003	< 0.02
Gd	0.005	< 0.09	< 0.04	< 0.003	0.004	< 0.12	0.014
Tb	< 0.003	0.007	< 0.01	< 0.003	< 0.01	< 0.02	< 0.01
Dy	0.009	0.035	0.014	0.004	< 0.05	< 0.07	< 0.12
Y	0.027	0.079	0.020	0.012	0.056	< 0.04	< 0.10
Ho	< 0.003	< 0.01	< 0.003	< 0.003	< 0.02	< 0.01	0.009
Er	0.003	< 0.41	< 0.25	0.003	< 0.12	< 0.59	< 0.64
Tm	< 0.003		< 0.01	< 0.003	< 0.07		
Yb	0.005	< 0.08	0.006	0.015	< 0.01	< 0.09	< 0.10
Lu	< 0.003	< 0.02	< 0.003	< 0.003	0.015	< 0.01	< 0.02
Li	2.30			1.81	1.30		3.64
Sc	20.3	2.57	2.42	18.4	3.12	2.33	2.20
V	6.92	8.01	5.36	6.23	4.83	4.52	4.26
Cr	184	253	132	175	220		89
Mn	990	1120	1110	870	1050	1040	1200
Co	152	168		132	95	153	181
Ni	2840	3230	2640	2340	2720	2930	3550
Cu		0.89			2.32	1.38	3.44
Zn	116	155	159	97	168	130	238
Ga	0.63	1.01		0.55	0.86	0.90	1.41

Table 3
Major and trace element analyses of orthopyroxene

wt.%	Gt-peridotites		Gt–Sp-peridotites		Sp-peridotites		Pyroxenite
	SF-93163	SF-93205	SG-96B13	SF-93174	SG-96B11	SF-93162	SF-93803
SiO_2	55.07	54.94	55.37	54.73	54.82	54.91	54.00
TiO2	0.17	0.12	0.17	0.17	0.18	0.32	0.46
Al_2O_3	4.33	4.01	4.02	5.27	3.72	3.92	4.69
MgO	32.87	32.33	32.85	31.95	33.22	32.34	30.57
FeO	6.45	6.10	6.02	6.47	6.16	6.64	8.59
CaO	0.94	0.96	0.83	1.23	0.73	0.85	0.81
Na_2O	0.21	0.18	0.15	0.18	0.10	0.23	0.55
K_2O		0.01		0.01	0.01		0.01
Total	100.66	99.34	100.19	100.82	99.50	99.94	100.15
n	3	3	2	4	3	2	2
ppm							
Cs							
Rb	< 0.03		< 0.18	< 0.03	< 0.28		
Ba	< 0.06		< 0.65	< 0.08	< 0.71		
Th	< 0.003	< 0.01	< 0.04	0.003	< 0.02	< 0.02	< 0.01
U	< 0.003	< 0.01	0.004	< 0.003	< 0.04	< 0.02	< 0.01
Nb	0.039	0.12	< 0.20	0.106	0.46	0.13	0.073
Ta	< 0.003	0.006	< 0.03	< 0.003	0.017	< 0.02	< 0.01
La	0.005	< 0.01	< 0.003	0.012	< 0.07	< 0.02	< 0.01
Ce	0.024	0.050	< 0.03	0.061	< 0.08	0.054	0.039
Pr	0.006	< 0.02	< 0.02	0.009	< 0.03	0.042	0.011
Sr	0.35	0.21	0.38	0.55	0.72	0.41	1.24
Nd	0.046	0.14	0.045	0.059	< 0.14	< 0.09	0.088
Sm	0.023	0.036	< 0.10	0.028	< 0.24	< 0.15	< 0.10
Zr	1.34	0.45	1.10	1.41	11.3	1.09	5.58
Hf	0.066	0.043	0.022	0.056	0.55	0.057	0.31
Eu	0.015	< 0.02	< 0.03	0.014	< 0.03	< 0.02	0.048
Gd	0.032	< 0.09	< 0.16	0.025	< 0.21	< 0.16	0.076
Tb	0.012	< 0.02	0.006	0.012	0.041	0.040	0.014
Dy	0.069	0.056	< 0.10	0.073	0.14	< 0.07	0.15
Y	0.31	0.19	0.19	0.36	0.45	0.13	0.50
Ho	0.011	0.019	< 0.02	0.012	< 0.03	< 0.01	0.020
Er	0.036	< 0.53	< 0.69	0.045	< 0.77	< 0.59	< 0.27
Tm	0.007		< 0.03	0.008	< 0.07		
Yb	0.036	< 0.06	< 0.16	0.032	< 0.11	< 0.09	< 0.06
Lu	0.006	0.005	< 0.003	0.004	< 0.02	< 0.01	< 0.01
Li	1.36			1.23			2.70
Sc	30.6	8.63	8.03	27.7	10.8	7.69	6.16
V	108	101	110	102	63.9	100	59.9
Cr	3650	3370	3510	3780	3860	4580	1280
Mn	960	1010	1030	910	1010	890	780
Co	62.7	68.4		56.4	55.3	55.8	53.5
Ni	810	800	880	670	790	720	730
Cu		0.97			3.55	1.04	2.52
Zn	73.8	93.8	97.6	61.1	100	68.2	91.0
Ga	6.71	6.45		6.49	5.69	6.72	9.5

1989; Menzies, 1990). The samples with the lowest modal olivine contents which plot to the right of the spinel lherzolite field in Fig. 4 are ‘‘re-fertilised’’ samples with high proportions of second-generation

Table 4
Major and trace element analyses of clinopyroxene

wt.%	Gt-peridotites		Gt–Sp-peridotites		Sp-peridotites	
	SF-93163	SF-93205	SG-96B13	SF-93174	SG-96B11	SF-93162
SiO_2	52.36	51.88	52.55	52.09	52.07	52.21
TiO_2	0.54	0.42	0.57	0.59	0.95	0.61
Al_2O_3	6.56	5.59	5.70	6.75	6.58	5.86
MgO	16.16	15.49	15.66	16.02	14.86	15.55
FeO	3.51	3.00	3.02	3.63	3.47	3.11
CaO	17.25	18.88	19.05	16.88	17.25	19.28
Na_2O	1.92	1.82	1.84	1.94	2.52	1.91
K_2O	0.01	0.02	0.01	0.01	0.01	0.01
Total	99.59	98.46	100.54	99.34	99.41	99.51
n	2	4	4	3	4	4
ppm						
Cs					< 0.01	
Rb	0.11		< 0.06	< 0.03		
Ba	0.17		< 0.10	0.105	0.085	
Th	0.011	< 0.003	0.022	0.113	0.081	0.037
U	0.005	< 0.01	0.0090	0.020	0.019	0.020
Nb	0.25	0.32	0.54	1.21	1.41	0.61
Ta	0.021	0.027	0.034	0.067	0.39	0.041
La	0.68	0.084	0.92	1.87	1.55	1.25
Ce	2.73	0.84	3.79	5.44	7.82	4.36
Pr	0.56	0.24	0.69	0.84	1.56	0.82
Sr	71.5	27.5	73.4	80.6	87.4	80.8
Nd	3.55	1.79	3.63	4.38	8.67	4.65
Sm	1.25	0.84	1.38	1.41	3.60	1.47
Zr	15.5	6.25	17.1	17.4	229	21.5
Hf	0.83	0.39	0.79	0.87	11.1	0.92
Eu	0.46	0.29	0.48	0.47	1.11	0.48
Gd	1.20	0.77	1.38	1.32	3.38	1.33
Tb	0.20	0.12	0.17	0.21	0.48	0.17
Dy	0.90	0.57	0.90	0.97	2.48	0.71
Y	3.50	2.21	2.99	3.54	7.98	2.06
Ho	0.17	0.106	0.11	0.16	0.38	0.102
Er	0.37	< 0.58	< 0.31	0.36	0.75	< 0.48
Tm	0.038		0.029	0.037	< 0.13	
Yb	0.24	0.103	0.17	0.22	0.32	0.097
Lu	0.029	0.012	0.017	0.030	0.048	0.013
Li	1.31			1.69		
Sc	33.4	26.4	30.6	35.3	49.3	32.5
V	221	282	299	268	209	299
Cr	6330	6710	6600	8280	9500	
Mn	613	697	744	645	746	601
Co	23.5	25.9		24.3	23.7	21.8
Ni	348	411	363	344	346	346
Cu		4.50			12.8	4.06
Zn	26.0	37.6	33.8	29.3	38.4	22.7
Ga	7.09	7.32		8.12	6.60	7.98

clinopyroxene. Olivine in the orthopyroxenites shows clearly lower Mg# of 86–87.

Orthopyroxenes are unzoned and also have Mg# ranging between 89 and 91, correlating with the

Table 5
Major and trace element analyses of garnet

wt.%	Gt-peridotites		Gt–Sp-peridotites	
	SF-93163	SF-93205	SG-96B13	SF-93174
SiO_2	42.49	41.71	42.40	43.06
TiO_2	0.21	0.16	0.18	0.21
Al_2O_3	22.92	23.33	22.57	22.67
MgO	21.53	20.79	21.01	21.79
FeO	7.44	7.17	7.17	7.36
CaO	4.79	4.92	4.95	4.79
Na_2O	0.02		0.02	0.03
K_2O	0.01			
Total	100.96	99.87	99.91	101.65
n	4	5	5	4
ppm				
Cs				
Rb	< 0.04		< 0.08	< 0.08
Ba	< 0.12		< 0.16	0.103
Th	< 0.003	< 0.003	< 0.003	0.005
U	0.003	0.010	< 0.01	0.007
Nb	0.13	0.21	0.22	0.20
Ta	0.008	< 0.02	< 0.01	0.006
La	0.004	< 0.02	0.013	0.019
Ce	0.066	0.020	0.067	0.12
Pr	0.030	< 0.02	0.023	0.036
Sr	0.18	0.16	0.15	0.24
Nd	0.39	0.14	0.23	0.39
Sm	0.58	0.28	0.37	0.59
Zr	20.7	6.82	13.0	22.5
Hf	0.42	0.16	0.24	0.45
Eu	0.37	0.19	0.23	0.34
Gd	1.30	0.94	1.05	1.32
Tb	0.51	0.26	0.30	0.46
Dy	4.20	2.15	2.40	3.75
Y	25.4	14.4	14.5	21.8
Ho	1.03	0.56	0.56	0.84
Er	3.30	1.58	1.71	2.54
Tm	0.49		0.23	0.35
Yb	3.36	1.83	1.52	2.25
Lu	0.51	0.27	0.21	0.34
Li	0.15			0.13
Sc	95.8	92.3	86.8	72.0
V	115	95.6	91.1	98.2
Cr	10,600	6720	6180	9160
Mn	2680	1980	2310	2290
Co	52.0	38.6		44.4
Ni	105	69.2	47.0	70.7
Cu		0.21		
Zn	39.9	33.5	31.1	27.7
Ga	6.15	4.02		4.93

Mg# in coexisting olivines. Correspondingly, the Mg# in the pyroxenites is 86–87. TiO_2 and Cr_2O_3 contents of orthopyroxenes are higher in spinel lherzolites than in either group of garnet-bearing peridotites, and also higher than typical spinel lherzolites from other localities around the world. The garnet-bearing samples, however, are similar to fertile spinel lherzolites from non-cratonic areas. The presence or absence of phlogopite and/or amphibole in the Bereya samples does not affect this observation. Compared to the other samples orthopyroxene in the cumulate pyroxenites contains less Cr_2O_3 but considerably more TiO_2 (0.45–0.5 wt.%; see Table 3, sample SF-93803).

Considering their varying textural relationships, clinopyroxenes in the Bereya peridotites are remarkably uniform in composition; they are diopsides with a high content of jadeiite (8.75–16.5 mol%) resulting from exceptionally high Na_2O contents, which are on average higher than all known spinel lherzolite localities. TiO_2 contents decrease from the spinel peridotites (0.6–1.1 wt.%) to the garnet peridotites (0.4–0.55 wt.%). The major element chemistry of the two clinopyroxene generations has been investigated thoroughly for samples SF-93163 and SF-93174, showing the second generation to have 0.4–0.5 wt.% higher Al_2O_3 (averages of 6.98 vs. 6.50 wt.% for SF-93174) and marginally lower Mg# (minimum of 88.2 vs. 88.9 in SF-93163), but to be otherwise essentially indistinguishable.

Garnets in the Bereya xenoliths are generally homogenous and pyrope-rich, with low contents of almandine, grossular and spessartine. Garnets in the garnet lherzolites have higher contents of CaO (5.22 vs. 4.75 wt.%) and Cr_2O_3 (1.5 vs. 1.05 wt.%) than in garnet–spinel lherzolites. Spinels are also uniform in composition, consisting of 54–61 mol% Mg-spinel, 15–18% hercynite, 15–21% Mg-chromite and 3–6% Fe-chromite. There are no significant differences in composition between spinel relicts in garnet and those which appear as individual grains, with the exception of two samples: spinel in the harzburgite sample SG-96B11 is richer in chromite component (30 mol%), while in sample SF-93163 (garnet lherzolite) the Mg-spinel component makes up 65 mol%. Spinels in kelyphites (Kp-2) are richer in Al_2O_3 than primary spinels.

Pargasitic amphibole occurring as inclusions in other silicate minerals in the spinel harzburgite has a higher Mg# (87), lower TiO_2 and higher K_2O than

Table 6
Major and trace element analyses of spinel

wt.%	Gt-peridotites		Gt–Sp-peridotites	Sp-peridotites	
	SF-93163	SF-93205	SG-96B13	SG-96B11	SF-93162
SiO_2	0.11	0.02	0.08	0.07	0.06
TiO_2	0.36	0.35	0.47	1.09	0.39
Al_2O_3	45.98	43.97	43.74	37.64	45.10
Cr_2O_3	19.33	22.72	22.52	26.30	20.61
MgO	18.63	18.55	18.51	17.22	18.46
FeO	13.36	13.26	13.71	16.10	13.64
CaO	0.02		0.02	0.04	
Na_2O					
K_2O	0.01		0.01	0.01	
Total	97.89	99.35	99.15	98.61	98.42
n	3	2	3	3	2
ppm					
Cs				< 0.49	
Rb	< 0.28		< 0.25	< 0.02	
Ba	< 0.55		< 0.64	< 0.04	
Th	< 0.003	0.002	0.021	0.018	< 0.04
U	< 0.003	< 0.002	0.008	< 0.003	< 0.07
Nb	1.18	1.28	4.59	3.98	2.91
Ta	0.008	0.069	< 0.11	< 0.01	< 0.07
La	0.004	< 0.003	< 0.07	< 0.003	< 0.06
Ce	0.004	0.072	< 0.06	0.017	< 0.10
Pr	< 0.003	0.032	< 0.06	< 0.003	< 0.12
Sr	0.17	0.20	0.29	< 0.78	0.66
Nd	0.021	< 0.003	0.092	< 0.02	< 0.16
Sm	< 0.003	< 0.003	0.077	< 0.02	< 0.20
Zr	0.80	3.31	2.87	3.35	3.05
Hf	0.018	< 0.01	0.46	0.12	0.11
Eu	< 0.003	< 0.003	< 0.07	< 0.003	< 0.07
Gd	0.004	0.45	0.039	< 0.03	< 0.50
Tb	< 0.02	0.021	< 0.04	< 0.003	< 0.05
Dy	0.009	0.008	< 0.21	< 0.02	< 0.25
Y	0.046	0.095	0.061	< 0.01	< 0.07
Ho	< 0.003	0.003	< 0.03	< 0.017	< 0.064
Er	0.013	< 0.003	< 2.02	< 0.15	< 1.68
Tm	0.003		< 0.06	< 0.01	
Yb	< 0.09	< 0.03	< 0.40	< 0.02	< 0.27
Lu	0.005	0.052	< 0.03	< 0.003	< 0.03
Li	0.61				
Sc	7.46	1.21	< 1.98	< 0.11	< 1.41
V	687	694	666	481	768
Mn	1070	950	1050	1110	1190
Co	252	418		254	273
Ni	3150	2730	2600	3960	3240
Cu		8.69		21.9	20.3
Zn	1350	1870	2310	2810	1950
Ga	139	116		97.9	146

in the pyroxenite (Mg# = 83). Both are enriched in Cr_2O_3 and K_2O relative to the vein amphiboles described by Ionov et al. (1993). Phlogopites occur rarely but are represented in all peridotite groups in

Table 7
Major and trace element analyses of amphibole and phlogopite

wt.%	Amphibole		Phlogopite		
	Sp-Lhz	Pyroxenite	Sp-Lhz	Gt–Sp-Lhz	Pyroxenite
	SG-96B11	SF-93803	SG-96B11	SG-96B13	SF-93803
SiO_2	42.87	41.76	38.08	38.46	35.66
TiO_2	3.41	4.38	4.60	4.62	6.57
Al_2O_3	13.24	13.76	15.11	15.88	16.21
MgO	16.62	16.23	19.91	20.23	18.63
FeO	4.45	5.88	4.57	4.31	6.53
CaO	9.78	8.41	0.30	0.03	0.04
Na_2O	3.02	3.58	0.49	0.41	1.16
K_2O	2.13	1.26	7.54	9.65	8.06
Total	97.33	96.21	92.22	95.15	93.56
n	5	2	3	3	1
ppm					
Cs			1.31		
Rb	5.95		154	41.4	
Ba	79.5		824	431	
Th	0.072	0.034	< 0.04	< 0.02	0.003
U	0.014	0.012	< 0.02	0.010	0.090
Nb	53.5	15.9	34.4	22.4	4.1
Ta	5.23	1.33	3.06	0.66	0.50
La	2.23	2.22		0.15	< 0.10
Ce	9.98	10.3	0.52	< 0.02	0.19
Pr	1.79	1.88		< 0.03	< 0.03
Sr	214	249	77.5	45.9	91.8
Nd	9.60	10.8	< 0.18	< 0.14	< 0.06
Sm	3.53	3.36	< 0.22	< 0.17	< 0.14
Zr	191	98.8	28.1	3.92	6.00
Hf	8.26	4.85	0.78	0.21	0.36
Eu	1.23	1.28	< 0.05	< 0.04	0.056
Gd	3.13	3.35	< 0.30	0.11	0.28
Tb	0.44	0.54	< 0.05	0.006	< 0.05
Dy	2.17	2.55		< 0.07	< 0.11
Y	6.81	9.04	0.78	0.35	1.36
Ho	0.28	0.40		< 0.02	< 0.02
Er	0.58	0.79	< 1.01	< 0.90	< 0.49
Tm	0.059			< 0.03	
Yb	0.34	0.32	< 0.25	0.084	< 0.13
Lu	0.040	0.032		< 0.003	< 0.03
Li		1.16	7.70		3.85
Sc	29.5	15.9	4.42	3.77	2.70
V	244	219	199	387	181
Cr	10,300	4200	9730	9040	2440
Mn	430	506	176	170	161
Co	35.4	42.0	63.1		63.8
Ni	814	829	2090	1660	1910
Cu	14.5	16.0	13.7		7.62
Zn	45.1	52.8	80.2	66.9	68.0
Ga	20.9	28.0	177		310

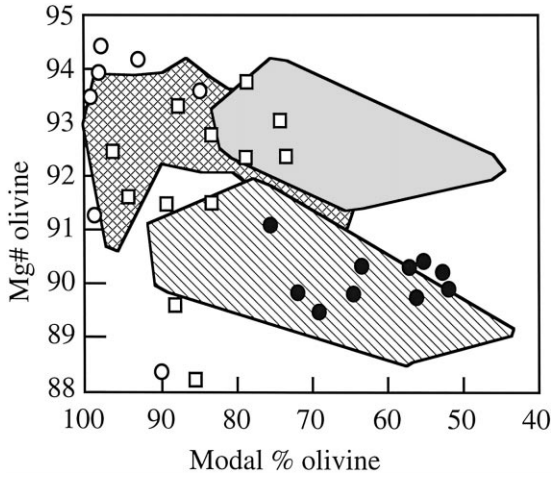

Fig. 4. Relation between Mg# of olivine and modal olivine content in peridotites from various areas. The Bereya samples (filled circles) fall mostly within the field characteristic for fertile spinel lherzolites (diagonally shaded field = Proterozoic samples after Menzies, 1990) and are distinct from the field of Kaapvaal cratonic peridotites, which are offset to higher Mg# at similar modal olivine contents (grey shading; Boyd, 1989). Depleted peridotites of Tanzania (Lashaine = squares, Olmani = open circles; Rudnick et al., 1994) and West Greenland (cross-hatch; Bernstein et al., 1998) lie to higher Mg# and modal olivine contents.

Bereya. Peridotitic phlogopites contain less TiO_2 but more Cr_2O_3 than those in the pyroxenite (Table 7) and have higher Mg# (89 vs. 84).

3.3. Pressure and temperature estimates for the peridotites

The infiltration of the peridotites by a silicate melt within the mantle and the resulting disequilibrium between major mineral phases poses problems for the selection of suitable thermometers and barometers. We have, therefore, compared the results from several thermometers, including (1) Ca-in-orthopyroxene, (2) Na exchange between pyroxenes, and (3) the commonly used ''two-pyroxene'' thermometer (diopside (Di)–enstatite (En) exchange between clinopyroxene and orthopyroxene). All formulations were those of Brey and Köhler (1990). Pressure was estimated by the orthopyroxene/garnet Al_2O_3 exchange barometer of Brey and Köhler (1990) for garnet-bearing samples, and by the Cr-in-spinel barometer of Webb and Wood (1986) for spinel-bearing samples. The latter barometer permits estimates for garnet-free samples from Bereya by elimination of Cr in garnet from the calculation.

The results give P–T estimates of 20–23 kbar and 1024°C–1087°C for the garnet lherzolites, 20–21 kbar and 1000°C–1034°C for the garnet–spinel lherzolites, and 20–22 kbar and 1005°C–1090°C for the spinel lherzolites. The results for the garnet-bearing samples are similar to the range of 16.5–22.5 kbar and 990°C–1150°C given by Ionov et al. (1993), and are all very close to the transition depth between spinel and garnet lherzolites. Similar depths for all xenolith types are also suggested by the occurrence of composite xenoliths (Ionov et al., 1993). A much larger pressure range of 18–30 kbar is given by Ashchepkov et al. (1994) and Litasov and Litasov (1999) on the basis of a more extensive sample collection, although using different thermobarometers.

The most reliable temperature estimates came from the Ca-in-orthopyroxene thermometer, probably because it does not consult the composition of the coexisting clinopyroxene which was disturbed or even fully introduced during the melt infiltration event. The Na-thermometer overestimates temperatures by variable amounts up to 300°C which result in absurdly high pressure estimates (up to 15 kbar too high) when combined with barometers. The Di–En thermometer also overestimates temperatures, but to a lesser extent (generally < 130°C). The overestimation by both thermometers using the clinopyroxene composition is considered to indicate disequilibrium between the pyroxenes, which finds its textural expression in Fig. 3c–f.

The temperatures for the sheared lherzolite (1005°C by Ca-in-orthopyroxene) are severely *underestimated* by the other two thermometers (620°C by the Di–En exchange thermometer). The reason for this is not clear, but it cannot be a simple function of the high jadeite contents, which are also higher in other Bereya samples relative to peridotites from other areas. In contrast to a sheared peridotite reported by Ashchepkov et al. (1994) and to sheared garnet peridotites sampled by kimberlites (Nickel and Green, 1985), the temperature estimates for the sheared sample are not higher than for undeformed samples.

4. Trace element chemistry of minerals

Seven samples were selected for trace element analysis by Laser Ablation Microprobe (LAM–ICP-MS) to provide representative information on the trace element behaviour of each of the three xenolith groups. These seven samples include two with textural evidence for melt infiltration, the sheared xenolith SF-93162, and an amphibole- or phlogopite-bearing example of each group, where available.

The Laser–ICP-MS system used was that at the ETH in Zürich, Switzerland, which consists of an Excimer laser coupled to a Perkin-Elmer ELAN 6000 ICP-MS (Günther et al., 1997). The ICP-MS is equipped with a dual detector mode, allowing simultaneous detection of major and trace elements, so that almost all major elements were monitored during analysis of a trace element palette of up to 40 elements. The prototype excimer laser (5% F in Ar, 193 nm) beam is homogenised, allowing very homogeneous laser illumination of the sample surface and control of the ablation process. Fractionation effects are reduced to an insignificant amount by the photoionisation-dominated ablation process, so that accuracy is better than 5% even for highly fractionating elements. This is especially valuable for the more volatile compatible trace elements such as Zn and Ga. Reproducibility is sample-dominated; 10 replicates on homogeneous test samples allow relative standard deviations of 1–3% for most of the elements. Signal correlation between volatile and refractory elements shows no significant fractionation effects until ablation pit depth exceeds pit diameter. This posed no problem for the analyses presented here, which were performed with pit diameters of 40–80 μm on marginally thick polished thin sections using pulse energies of 120–200 mJ and a repetition rate of 10 Hz. The analyses were standardised externally on NIST 610 and 612 glasses, and internally on electron probe analyses of Si for silicate phases and Al for spinels. For data acquisition parameters and data reduction procedure used for the calculation of concentrations and limits of detection see Longerich et al. (1996).

We have analyzed incompatible (ITE) as well as compatible (CTE) trace elements in all constituent phases (olivine, orthopyroxene, clinopyroxene, garnet, spinel, amphibole and phlogopite). As a result of the optimized laser system we can present a more complete set of partitioning data for minerals with very low concentrations of many trace elements (e.g., spinel and orthopyroxene), and for mineral pairs (e.g., garnet/spinel) than was previously possible using in situ techniques. Results are listed in Tables 2–7 for individual minerals and illustrated in Figs. 5–7. Arsenic is not listed in the tables as it was detected only in one spinel in a garnet lherzolite at a level of 0.12 ppm. The limits of detection for all other measured isotopes are in the very low 1–10 ppb region even for a spatial resolution of 40 μm. These low limits of detection are mainly due to changes in the carrier gas composition leading to increased sensitivity and reduced background intensities. A 300 ml/min helium carrier gas flow through the ablation cell was mixed with argon in front of the ICP-MS to maintain the total gas flow at an optimum level (Günther and Heinrich, 1998). For Li almost no background counts have been detected resulting in greatly improved detection capabilities for elements with low atomic mass.

4.1. Incompatible trace elements

ITE abundances are illustrated in Fig. 5 for orthopyroxene, clinopyroxene, garnet and amphibole. No plots are presented for olivine, spinel and phlogopite as the patterns are incomplete despite the very low limits of detection of the Laser–ICP-MS.

Fig. 5a compares the patterns for the Bereya orthopyroxenes to a pattern for an orthopyroxene mineral separate from a xenolith from the Baikal Rift-related Tariat volcanic field in Mongolia (Ionov and Hofmann, 1995) and to a Laser–ICP-MS analysis from a spinel lherzolite from southeastern Australia (Eggins et al., 1998). Although the patterns are generally similar, the abundances of Nb, Ta and Th detected in the Bereya samples are significantly higher than in the patterns for the other two localities. The patterns for garnet also show higher abundances for elements to the left of La in Fig. 5c than are expected from experimentally determined partition coefficients (Green, 1994). In contrast, the patterns for clinopyroxene and amphibole (Fig. 5b and d) generally correspond to those expected for these minerals in peridotites. The ITE patterns are interpreted as showing variable degrees of approach to

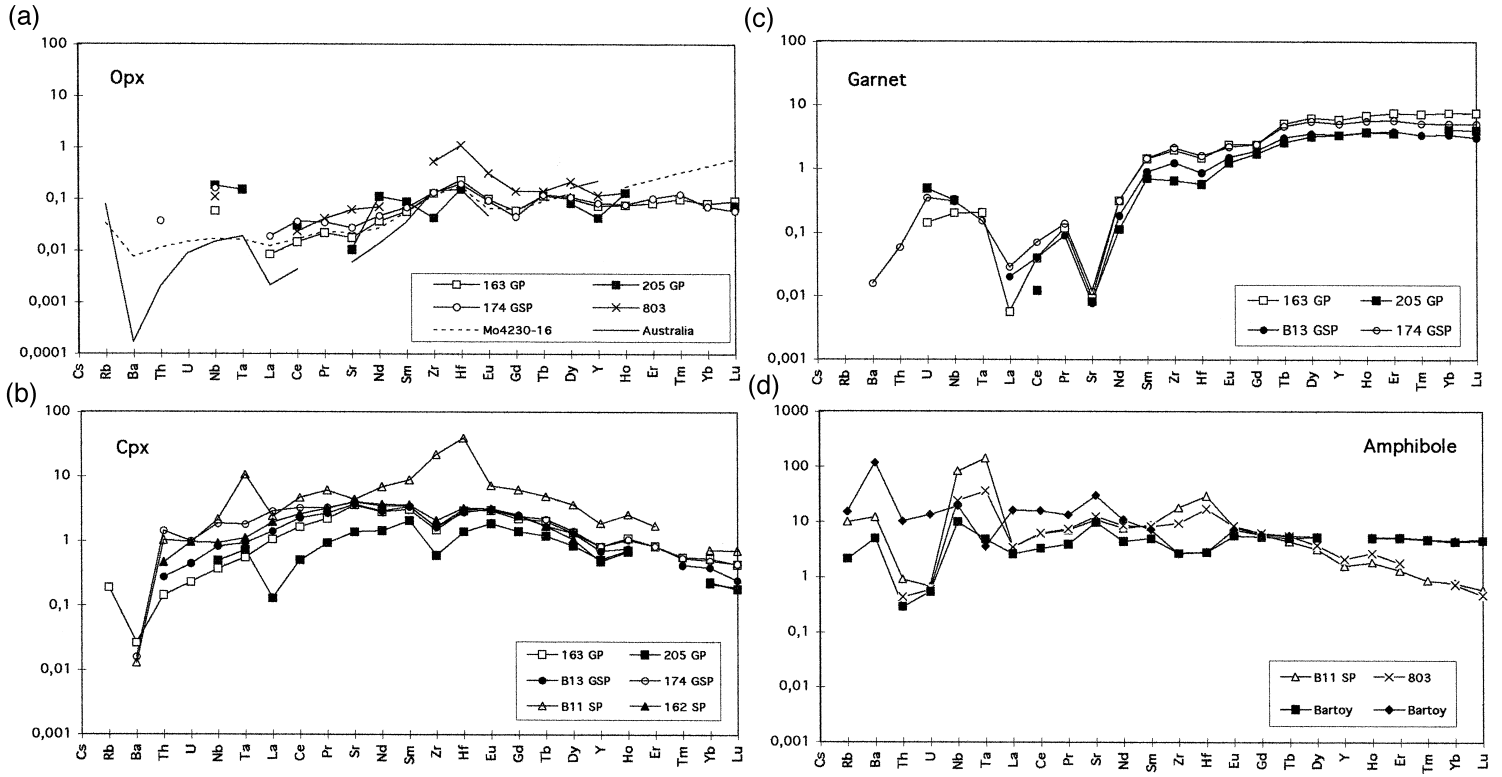

Fig. 5. Incompatible trace elements in minerals from Bereya peridotites normalised to primitive mantle using values given by Sun and McDonough (1989). (a) Orthopyroxene: overall levels are typical for peridotitic orthopyroxene for the less incompatible elements (right of diagram) but the more incompatible elements (left) are unusually enriched indicating partial re-equilibration with infiltrating melt. The Tariat sample (+; Ionov and Hofmann, 1995) is also from the Baikal region (see Fig. 1) but does not show this enrichment. The solid line indicates Opx from spinel lherzolites from southeastern Australia (Eggins et al., 1998). Only samples where 12 or more ITE were detected are plotted. (b) Clinopyroxene patterns are notable for inconsistent behaviour of HFSE. (c) Garnets show normal patterns to the right of Sr, but unusual enrichments to the left, indicating partial re-equilibration with infiltrating melt. (d) Amphiboles differ from those of Bartoy (Ionov and Hofmann, 1995; see Fig. 1), with lower HREE and higher HFSE, reversing the sense of the anomaly for Zr and Hf.

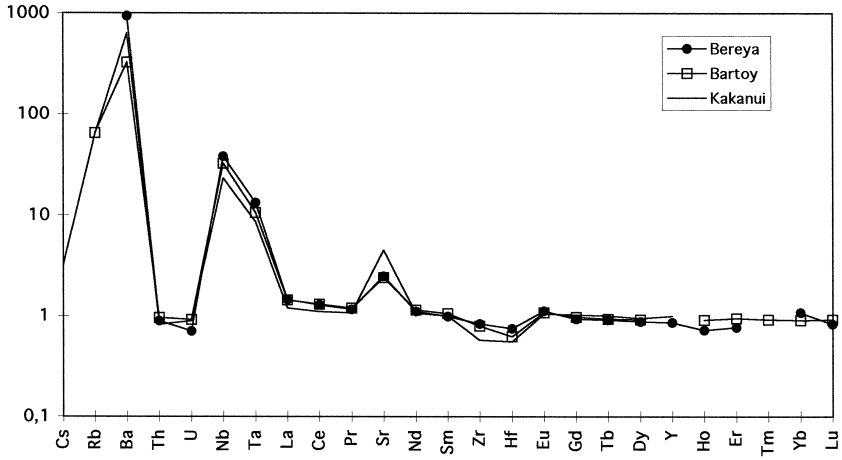

Fig. 6. Amphibole/clinopyroxene partitioning of trace elements, showing similar patterns for Bereya to those for Kakanui garnet pyroxenites (Zack et al., 1997) and Bartoy xenoliths (Ionov and Hofmann, 1995). Similarity of patterns is evidence for ITE equilibrium between these two phases in the Bereya peridotites.

equilibrium for ITE in different minerals, whereby only the strongly incompatible elements in orthopyroxene and garnet have responded to the infiltrating melt. The degree of re-equilibration is much greater for clinopyroxene and amphibole, and amphibole/clinopyroxene partitioning is similar to that found in other areas (Fig. 6) supporting the interpretation that these two minerals are in ITE equilibrium with each other.

The ITE patterns for clinopyroxene and amphibole are also noteworthy for the behaviour of Nb, Ta, Zr and Hf. Most clinopyroxenes show a trough in the pattern at Zr and Hf, which is a well-known feature of peridotitic clinopyroxenes (Salters and Shimizu, 1988; Rampone et al., 1991), whereas SG-96B11 shows positive anomalies for Zr, Hf and even Ta (Fig. 5c). Both the analysed amphiboles (from spinel harzburgite SG-96B11 and the pyroxenite SF-93803) show strong positive anomalies in the pattern at Zr–Hf and Nb–Ta. The Zr–Hf anomalies are not evident in amphiboles analysed by Ionov and Hofmann (1995) from Bartoy, whereas the ratios amphibole/clinopyroxene shown in Fig. 6 are very similar to those from Bartoy and to garnet clinopyroxenites from Kakanui in New Zealand (Zack et al., 1997).

The improved Laser–ICP-MS system allowed analysis of Li in several phases. The results confirm those of Ottolini and McDonough (1996) that olivine is more enriched in Li than the pyroxenes and spinel, but add the observation that phlogopite would be more enriched in Li than olivine in hydrous mantle peridotites, albeit marginally. The Bereya phlogopites show significantly lower Li/Nb than those analysed in natural lamprophyres (Foley et al., 1996) or in experimental partitioning studies (Schmidt et al., 1998); olivine was not present in either of the latter studies. Spinel analyses show very low levels of most ITEs (0.01–0.2 times primitive mantle) but appreciably more of the high field strength elements (HFSE), and are consistent with other data for low-Ti spinels (Stosch, 1982; Horn et al., 1994).

4.2. Compatible trace elements

The Excimer Laser–ICP-MS system enabled the analysis of an extensive data set for CTE in all phases in the xenoliths. The values of Mn, Cr and Ni are comparable with those measured by microprobe (e.g., Ni in SG-96B11: 2720 ppm by LAM vs. 3080 by EMP; in SF-93162: 2930 vs. 3070; in SF-93163: 2840 vs. 2860). Values for the CTE are also given in Tables 2–7, and their relative concentrations in the mineral phases are illustrated in Fig. 7. Previous data sets have analyses for fewer CTE, and very few of them include garnet-bearing lherzolites (Stosch, 1981; Luhr and Aranda-Gómez, 1997; Qu et al.,

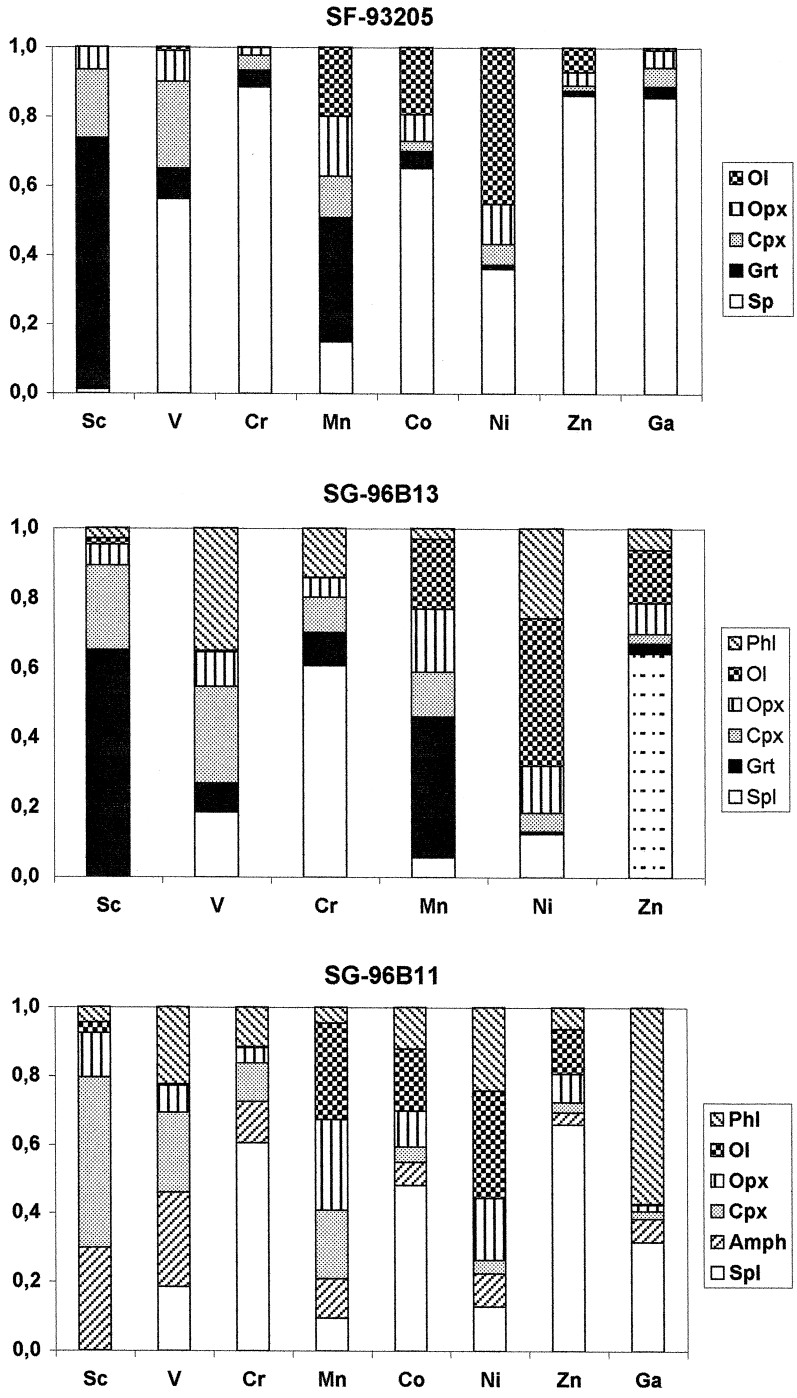

Fig. 7. Distribution of compatible trace elements between the phases of representative Bereya garnet lherzolites (SF-93205), garnet–spinel lherzolites (SG-96B13) and spinel harzburgite SG-96B11. The latter two samples also contain hydrous phases. Garnet is the main carrier for Sc and marginally so for Mn. Spinel is the dominant carrier of Cr, Co and Zn, and also for Ga in the absence of phlogopite.

1997; Eggins et al., 1998). In making comparisons it must be remembered that the constituent minerals of the Bereya peridotites are not all in equilibrium with each other, and that partitioning of many of these elements is known to be a strong function of temperature, so that the temperature recorded by these xenoliths (1050 ± 50°C) must be taken into account.

Fig. 7 shows that in garnet lherzolite SF-93205 garnet has the highest concentrations of Sc, whereas spinel dominates V, Cr, Co, Zn and Ga. Appreciable concentrations of Mn are found in all lherzolite phases, but are highest in garnet, where present. Ni is carried by olivine and spinel in approximately equal amounts (3230 vs. 2730 ppm), whereby olivine dominates the total Ni budget due to its high modal abundance. The D_{Ni} (ol/opx) varies between 3.5 and 4.0 for the garnet peridotites and between 1.75 and 4.1 (average 3.53) for the whole lherzolite suite. Minerals have the aptitude to greatly influence element budgets in rocks where they are not major constituents only where the primitive mantle-normalised concentrations of these CTE are greater than about five. This is not the case for any CTE in either clino- or orthopyroxene, and is only marginally the case for Ni in olivine, Sc in garnet, and Ga in amphibole. Ga in phlogopite, and Zn, Ga, Cr and possibly V in spinel, however, can have 10–100 times the concentration of primitive mantle, so they cannot be neglected even when present in very small amounts.

The takeup of V in spinel is a strong function of oxygen fugacity because V^{3+} can be easily accommodated in spinel, whereas V^{5+}, which predominates under oxidising conditions, is incompatible in spinel (Horn et al., 1994). Calculation of the oxygen fugacity in Bereya peridotites gives values of FMQ to FMQ-1 (Ballhaus et al., 1991; Ionov and Wood, 1992), corresponding to DV (sp/cpx) in the range 2.2–2.6 (Horn et al., 1994). The Bereya peridotites also provide a rare opportunity to assemble a partitioning database for both ITE and CTE between coexisting garnet and spinel. Spinel contains very low abundances of ITE, resulting in a pattern for gt/sp resembling that of garnet. No anomaly is seen at Zr despite the preferential incorporation of Zr in spinel relative to the neighbouring ITEs because garnet also shows a small positive anomaly in its pattern (Fig. 5c).

5. Discussion

5.1. The melt infiltration event in the Bereya peridotites

The Bereya lherzolite sample suite studied here contains more evidence for trace element enrichment by melt infiltration within the mantle than described by Ionov et al. (1993) for samples from this locality. The combination of in situ trace element analyses of minerals with petrographic observations and major element chemistry permit the relative timing and conditions of the infiltration event to be defined, and also the nature of the infiltrating melt. This information helps to delineate the development of the mantle beneath the evolving Baikal rift.

The petrographically observed textures, including clinopyroxene networks which mimic melt morphologies (Fig. 3c–f) demonstrate the later crystallisation of clinopyroxene relative to garnets, spinels and many olivines and orthopyroxenes, and that the clinopyroxene crystallised from an infiltrating melt. Given this evidence for strong textural disequilibrium, it may be suspected that chemical equilibration between previously existing minerals and the infiltrating melt was also not reached and that disequilibrium partitioning occurs. There are several indications for only a partial attainment of equilibrium: (1) the anomalously high contents of the most incompatible elements in orthopyroxenes and especially garnets (Fig. 5a and c) may indicate that these minerals were affected by the infiltrating melt but that equilibrium was not reached; (2) the patterns for clinopyroxene (Fig. 5b) and amphibole (Fig. 5d) lack the anomalous relative enrichment in the strongly incompatible elements, being consistent instead with equilibrium trace element distribution with the melt and with each other (Fig. 6); (3) the application of thermobarometers incorporating clinopyroxene compositions result in misleading temperature estimates, whereas those made using only orthopyroxene are probably realistic.

We interpret these features as indicating that the ITE abundances in orthopyroxene and garnet show some effects of interaction with the infiltrating melt, whereas their major and CTE abundances are largely unaffected. There is some evidence for the existence of an earlier clinopyroxene generation in the form of

minor zonation in Al_2O_3 and Mg# and also in zonation of ITE towards patterns more enriched in all ITE (these rare analyses are not included in the averages in Table 4 or in Fig. 5b). However, even the earliest clinopyroxenes are unlikely to represent unchanged, pre-infiltration compositions, as indicated by the failure of the thermometers. Thus, the apparently very fertile compositions of the Bereya peridotites (Fig. 4, Table 1) may be at least partly due to secondary introduction of melt components.

We have attempted to reconstruct the chemical identity of the infiltrating melt via experimental mineral/melt partitioning. This method assumes equilibrium between minerals currently found in the peridotite and the infiltrating melt, and that their ITE partitioning follows that determined in experimental work. This method must be considered crude in view of possible subsolidus re-equilibration of the ITE (Rampone et al., 1993; Eggins et al., 1998), but the preservation of ITE zonation justifies it as a first-order calculation.

Results of such calculations based on clinopyroxene from three samples and amphibole from a fourth are shown in Fig. 8 together with the trace element pattern for the host Miocene alkali picrite tuff (Esin et al., 1995) and a Quaternary basalt from the Vitim volcanic field (Ionov and Hofmann, 1995). The calculated melt from all three clinopyroxenes is similar to the natural volcanic patterns, whereas that for the amphibole deviates strongly for the HFSE. However, this is not due the use of inappropriate partition coefficients for these elements, which can be expected to vary as a function of the Ti-content of the melt (Tiepolo et al., 1998), but is a characteristic of sample SG-96B11; a similar pattern results when calculated from clinopyroxene. The sample-specificity of the positive anomaly for HFSE implies a very local effect, which is reminiscent of the extremely variable Zr concentrations found in clinopyroxenes of the Inagli complex, Siberia, by Zinngrebe et al. (1995). These authors attributed positive Zr anomalies to local reaction between infiltrating melt and spinels in the host ultramafic rocks. The anomaly is caused by the uptake of Al_2O_3 from spinel by the infiltrating melt which thus loses its peralkaline nature. In moving from peralkaline to subalkaline melt compositions the solubility of Zr in the melt drops sharply due to the elimination of alkali–Zr–silicate complexes which are only stable in peralkaline conditions (Watson and Harrison, 1983). The Bereya sample which shows the positive HFSE anomalies has the highest modal spinel (1.3 vol.%) and lowest

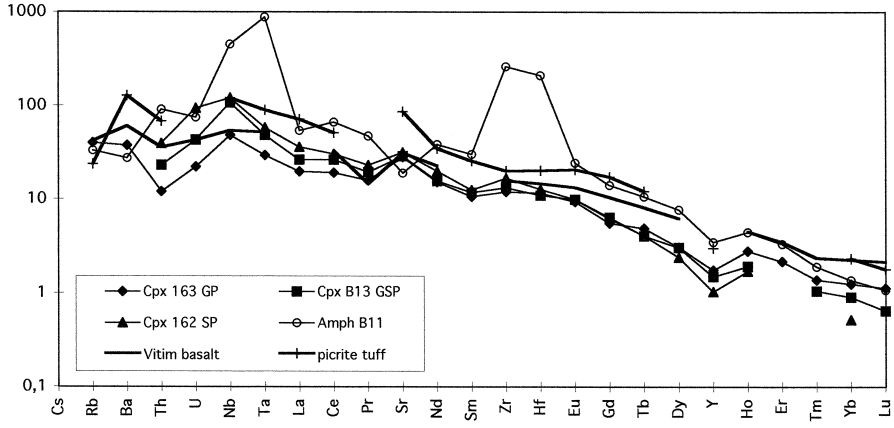

Fig. 8. Estimated ITE patterns of the infiltrating melt calculated by assuming that clinopyroxene and amphibole ITE-contents represent equilibrium values coexisting with the infiltrating melt. Patterns for cpx are obtained via mineral/melt partition coefficients after Watson et al. (1987), Adam et al. (1993), Hart and Dunn (1993), Jenner et al. (1993), Dalpé and Baker (1994), and Foley et al. (1996) as summarised by Zack et al. (1997), and amphibole after Zack et al. (1997). The pattern for the Bereya alkali picrite tuff is from the work of Esin et al. (1995), but may be suspected for some elements (e.g., Ba, Sr) due to the difficulty of obtaining fresh samples. However, this and an additional Vitim basalt from the Kandidushka volcano (sample 302-36; Ionov and Hofmann, 1995) show that the overall pattern for the melts calculated from Cpx is similar to that of volcanics from the same region. The pattern calculated from amphibole (B11) has positive anomalies which are characteristic of this sample (also Cpx) and not due to calculation via inappropriate partition coefficients.

modal clinopyroxene (0.5 vol.%) contents of any of the studied samples (Table 1) and so may represent the earlier stages of melt infiltration which are more likely to show strong effects of reaction with the host rock.

The similarity between the melt patterns calculated from clinopyroxene in Fig. 8 to the alkali picrite host indicates that the infiltrating melt may be related genetically to the host melt, and probably represents a marginally earlier stage in the history of the developing rift. The occurrence of rare ITE-richer zones in clinopyroxene probably indicate that the infiltrating melt was a lower-degree melt with peralkaline chemistry relative to the host alkali picrite.

5.2. Timing of events and the development of the Baikal Rift

The petrographic and mineral chemical information obtained from the Bereya peridotites allows delineation of events within the mantle at the southeast flank of the developing rift before the eruption event at 16 Ma. The effect of the rifting process within the mantle will have comprised a progressive upward and outward movement of the lithosphere/asthenosphere boundary, which was accompanied by the episodic infiltration of melts into the subcrustal lithosphere and their reactivation shortly afterwards by progressive development of the rift. The following series of events can be inferred from features in the peridotites.

(1) The peridotites underwent a reaction which formed garnet at the expense of spinel and pyroxenes, which is explainable by a near-isobaric cooling at pressures of 20–25 kbar. This may represent the lithosphere-forming event or possibly a later cooling event following perturbation of normal thermal conditions, but is in either case likely to pre-date the activity of the Baikal Rift.

(2) The outer reaction coronas around garnets (designated Kp-2 above) indicate a later heating event which we interpret as rift-related heating due to progressive upward and outward migration of the asthenosphere/lithosphere boundary between 30 and 15 Ma. The Kp-2 reaction coronas occasionally occur between the more continuous Kp-1 and the recrystallised rims of Cpx-2 clinopyroxenes. The latter two features are interpreted to have formed during uplift to the Earth's surface, whereas the Kp-2 rims must have existed prior to this, and most probably before the formation of Cpx-2 from the infiltrating melt. Furthermore, the mineralogy of the kelyphite indicates a reversal of the garnet-building reaction mentioned above, and implies Kp-2 kelyphite formation by a heating event in isochemical conditions, which is consistent with the upward and outward migration of the rift margin within the upper mantle.

(3) The melt infiltration event demonstrated by the textures in Fig. 3c–f post-dated the rift-related heating event indicated by the Kp-2 kelyphites, and was, therefore, directly related to heating at the flanks of the developing rift. The textures shown in Fig. 3e–f must be short lived: although the timescales for the attainment of textural equilibrium are controversial, the timescale for the elimination of the low angle-texture in Fig. 3e–f would certainly be less than 0.2 Ma, indicating melt infiltration very shortly before transport of the peridotites to the Earth's surface.

The peralkaline and ITE-rich chemistry of the melt inferred from the calculations presented above is consistent with its origin from the migrating rift within the mantle. Shortly after this melt infiltration, remelting of the enriched peridotites by a further heating event produced the alkali picrite melt which now hosts the peridotites at Bereya.

5.3. Comparison of non-cratonic and cratonic peridotites

The results presented here on the garnet-bearing peridotites from Bereya underline the general conclusion of Ionov et al. (1993) that the upper mantle in the garnet peridotite field in this non-cratonic, rift-related setting is distinct from that seen under cratonic regions in either South Africa or Siberia. The Bereya peridotites are fertile, with high modal abundances of clinopyroxene and garnet, and the relation between Mg# of olivine and modal olivine content is consistent with variable but limited depletion by loss of a basaltic melt fraction (Fig. 4). This conclusion is little modified by subsequent crystallisation of secondary clinopyroxene. The Bereya peridotites do not show a correlation between Ni content in olivine and modal orthopyroxene which is charac-

teristic of Kaapvaal cratonic lherzolites (Kelemen and Hart, 1996; Boyd, 1997).

Sheared lherzolite SF-93162 illustrates further differences between the Bereya peridotites and their cratonic counterparts: this xenolith exhibits a mosaic texture (Fig. 4b) but does not show the fluidal mosaic texture typical of sheared peridotites from cratonic regions (Boullier and Nicolas, 1975). Moreover, thermobarometric estimates do not deviate from those of the granular peridotites. Taken together, these points may indicate a different origin of the shearing as unrelated to the movement of magma or diapirs in the mantle, to which kimberlitic sheared xenoliths are often attributed (e.g., Ehrenberg, 1979; Mercier, 1979). Maybe this xenolith is an example of ''cold'' shearing related to the widening of the rift at its flanks, and thus similar to the origin originally suggested for kimberlitic sheared xenoliths (Nixon et al., 1973) but which subsequently fell out of favour.

Acknowledgements

The xenoliths described here were collected by the authors in 1993 and 1996 during fieldwork orchestrated by Igor Ashchepkov. Financial assistance for the fieldwork was provided by the Deutsche Forschungsgemeinschaft (Fo 181/3-1/3-2). We are grateful to S. Schmidberger and W.F. McDonough for reviews of the manuscript, and to K. Litasov, I. Ashchepkov, E. Zinngrebe, D. Ionov, M. Drury, U. Faul and H. Green for fruitful discussions and comments. Bill McDonough is also thanked for generously sharing his database on peridotitic xenoliths.

References

Adam, J., Green, T.H., Sie, S.H., 1993. Proton microprobe determined partitioning of Rb, Sr, Ba, Y, Zr, Nb and Ta between experimentally produced amphiboles and silicate melts with variable F-content. Chemical Geology 109, 29–49.

André, L., Ashchepkov, I.V., 1996. Acid leaching experiments on the mantle-derived Vitim clinopyroxenes: implications for the role of clinopyroxenes in the mantle processes. In: Demaiffe, D. (Ed.), Petrology and Geochemistry of Magmatic Suites of Rocks in the Continental and Oceanic Crusts. Royal Museum for Central Africa, Univ. Libre de Bruxelles, pp. 321–336.

Andronikov, A.V., 1990. Spinel–garnet lherzolite nodules from alkaline–ultrabasic rocks of Jetty Peninsula (East Antarctica). Antarctic Science 2, 321–330.

Andronikov, A.V., Foley, S.F., Melzer, S., 1998. Mantle xenoliths from the Jetty Peninsula area (East Antarctica): samples of thermally eroding lithosphere on the flanks of the Lambert–Amery rift. Extended Abstract 7th International Kimberlite Conference, Cape Town, pp. 20–22.

Ashchepkov, I.V., Litasov, Y.D., Dobretsov, N.L., 1994. Pyroxenites and composite garnet peridotite xenoliths from picrite–basalt, Vitim Pltaeau (Transbaikal): implications for thermobarometry and mantle reconstruction. In: Meyer, H.O.A., Leonardos, O.H. (Eds.), Kimberlites, Related Rocks and Mantle Xenoliths. CPRM Special Publ., Brasilia, pp. 455–466.

Ballhaus, C., Berry, R.F., Green, D.H., 1991. High pressure experimental calibration of the orthopyroxene–spinel oxygen geobarometer: implications for the oxidation state of the upper mantle. Contributions to Mineralogy and Petrology 107, 27–40.

Bernstein, S., Kelemen, P.B., Brooks, C.K., 1998. Depleted spinel harzburgite xenoliths in Tertiary dykes from East Greenland: restites from high degree melting. Earth and Planetary Science Letters 154, 221–235.

Boullier, A.M., Nicolas, A., 1975. Classification of textures and fabrics of peridotite xenoliths from South African kimberlites. Physics and Chemistry of the Earth 9, 467–476.

Boyd, F.R., 1989. Compositional distinction between oceanic and cratonic lithosphere. Earth and Planetary Science Letters 96, 15–26.

Boyd, F.R., 1997. Correlation of orthopyroxene abundance with the Ni content of coexisting olivine in cratonic peridotites. EOS Transactions of the American Geophysical Union 78, F746.

Boyd, F.R., Pokhilenko, N.P., Pearson, D.G., Mertzman, S.A., Sobolev, N.V., Finger, L.W., 1997. Composition of the Siberian cratonic mantle: evidence from Udachnaya peridotite xenoliths. Contributions to Mineralogy and Petrology 128, 228–246.

Brey, G.P., Köhler, T., 1990. Geothermobarometry in four-phase lherzolites: II. New thermobarometers, and practical assessment of existing thermobarometers. Journal of Petrology 31, 1353–1378.

Cao, R.-L., Zhu, S.-H., 1987. Mantle xenoliths and alkali-rich host rocks in eastern China. In: Nixon, P.H. (Ed.), Mantle Xenoliths. Wiley, New York, pp. 167–180.

Cmíral, M., FitzGerald, J.D., Faul, U.H., Green, D.H., 1998. A close look at dihedral angles and melt geometry in olivine–basalt aggregates: a TEM study. Contributions to Mineralogy and Petrology 130, 336–345.

Dalpé, C., Baker, D.R., 1994. Partition coefficients for rare earth elements between calcic amphibole and Ti-rich basanitic glass at 1.5 Gpa, 1100°C. Mineralogical Magazine 58A, 207–208.

Dawson, J.B., 1980. Kimberlites and their Xenoliths. Springer, Berlin, 252 pp.

Eggins, S.M., Rudnick, R.L., McDonough, W.F., 1998. The composition of peridotites and their minerals: a laser-ablation ICP-MS study. Earth and Planetary Science Letters 154, 53–71.

Ehrenberg, S.N., 1979. Garnetiferous ultramafic inclusions in

minette from the Navajo volcanic field. In: Boyd, F.R. Meyer, H.O.A. (Eds.), The Mantle Sample: Inclusions in Kimberlites and Other Volcanics. American Geophysical Union, Washington, pp. 330–344.

Esin, S.V., Ashchepkov, I.V., Ponomarchuk, V.A., 1995. Petrogenesis of alkaline basaltoids from the Vitim plateau (Baikal Rift Zone). UIGGM, Siberian Branch, Russian Academy of Sciences Press, Novosibirsk, 58 pp.

Faul, U.H., 1997. Permeability of partially molten upper mantle rocks from experiments and percolation theory. Journal of Geophysical Research 102, 10299–10311.

Foley, S.F., Jackson, S.E., Fryer, B.J., Greenough, J.D., Jenner, G.A., 1996. Trace element partition coefficients for clinopyroxene and phlogopite in an alkaline lamprophyre from Newfoundland by LAM–ICP-MS. Geochimica et Cosmochimica Acta 60, 629–638.

Frey, F.A., Prinz, M., 1978. Ultramafic inclusions from San Carlos, Arizona: petrologic and geochemical data bearing on their petrogenesis. Earth and Planetary Science Letters 38, 129–176.

Green, T.H., 1994. Experimental studies of trace element partitioning applicable to igneous petrogenesis — Sedona 16 years later. Chemical Geology 117, 1–36.

Günther, D., Heinrich, C.A., 1998. Enhanced sensitivity in LAM–ICP-MS using helium as carrier gas. Submitted.

Günther, D., Frischknecht, R., Heinrich, C.A., Kahlert, H.-J., 1997. Capabilities of an ArF 193 nm excimer laser for LAM–ICP-MS. Journal of Analytical Atomic Spectrometry 12, 939–944.

Hart, S.R., Dunn, T., 1993. Experimental cpx/melt partitioning of 24 trace elements. Contributions to Mineralogy and Petrology 113, 1–8.

Harte, B., 1983. Mantle peridotites and processes — the kimberlite sample. In: Hawkesworth, C.J., Norry, M.J. (Eds.), Continental Basalts and Mantle Xenoliths. Shiva, Nantwich, pp. 46–91.

Horn, I., Foley, S.F., Jackson, S.E., Jenner, G.A., 1994. Experimentally determined partitioning of high field strength and selected transition elements between spinel and basaltic melt. Chemical Geology 117, 193–218.

Hunter, R.H., Taylor, L.A., 1982. Stability of garnet from the mantle: glass as evidence of metasomatic melting. Geology 10, 617–620.

Ionov, D.A., Hofmann, A.W., 1995. Nb–Ta-rich mantle amphiboles and micas: implications for subduction-related metasomatic trace element fractionations. Earth and Planetary Science Letters 131, 341–356.

Ionov, D.A., Wood, B.J., 1992. The oxidation state of subcontinental mantle: oxygen thermobarometry of mantle xenoliths from central Asia. Contributions to Mineralogy and Petrology 111, 179–193.

Ionov, D.A., Kramm, U., Stosch, H.-G., 1992. Evolution of the upper mantle beneath the southern Baikal Rift zone: an Sr–Nd isotope study of xenoliths from the Bartoy volcanoes. Contributions to Mineralogy and Petrology 111, 235–247.

Ionov, D.A., Ashchepkov, I.V., Stosch, H.-G., Witt-Eickschen, G., Seck, H.A., 1993. Garnet peridotite xenoliths from the Vitim volcanic field, Baikal region: the nature of the garnet–spinel peridotite transition zone in the continental mantle. Journal of Petrology 34, 1141–1175.

Jenner, G.A., Foley, S.F., Jackson, S.E., Green, T.H., Fryer, B.J., Longerich, H.P., 1993. Determination of partition coefficients for trace elements in high pressure–temperature experimental run products by laser ablation microprobe–inductively coupled plasma-mass spectrometry (LAM–ICP-MS). Geochimica et Cosmochimica Acta 57, 5099–5103.

Kelemen, P.B., Hart, S.R., 1996. Silica enrichment in the continental lithosphere via melt/rock interaction. Journal of Conference Abstracts 1, 308.

Kiselev, A.I., 1987. Volcanism of the Baikal Rift zone. Tectonophysics 142, 235–244.

Kiselev, A.I., Popov, A.M., 1992. Asthenospheric diapir beneath the Baikal Rift: petrological constraints. Tectonophysics 208, 287–295.

Litasov, K.D., Litasov, Yu.D., 1999. Evolution of mantle magmatism beneath the Vitim volcanic field (East Siberia). Proceedings of the Seventh International Kimberlite Conference. In press.

Logatchev, N.A., Zorin, Y.A., 1992. Baikal Rift zone: structure and geodynamics. Tectonophysics 208, 273–286.

Longerich, H.P., Jackson, S.E., Günther, D., 1996. Laser ablation inductively coupled plasma mass spectrometric transient signal data acquisition and analyte concentration calculation. Journal of Analytical Atomic Spectrometry 11, 899–904.

Luhr, J.F., Aranda-Gómez, J.J., 1997. Mexican peridotite xenoliths and tectonic terranes: correlations among vent location, texture, temperature, pressure, and oxygen fugacity. Journal of Petrology 38, 1075–1112.

Menzies, M., 1983. Mantle ultramafic xenoliths in alkaline magmas: evidence for mantle heterogeneity modified by magmatic activity. In: Hawkesworth, C.J., Norry, M.J. (Eds.), Continental Basalts and Mantle Xenoliths. Shiva, Nantwich, pp. 92–110.

Menzies, M., 1990. Archean, Proterozoic and Phanerozoic lithospheres. In: Menzies, M.A. (Ed.), Continental Mantle. Oxford Monographs 16, Oxford Science Publications, pp. 67–86.

Mercier, J.-C., 1979. Peridotite xenoliths and the dynamics of kimberlite intrusion. In: Boyd, F.R., Meyer, H.O.A. (Eds.), The Mantle Sample: Inclusions in Kimberlites and Other Volcanics. American Geophysical Union, Washington, pp. 197–212.

Mercier, J.-C., Nicolas, A., 1975. Textures and fabrics of upper mantle peridotites as illustrated by xenoliths from basalts. Journal of Petrology 16, 454–487.

Nickel, K.G., Green, D.H., 1985. Empirical geothermobarometry for garnet peridotites and implications for the nature of the lithosphere, kimberlites and diamonds. Earth and Planetary Science Letters 73, 158–170.

Nixon, P.H., 1987. Mantle Xenoliths. Wiley, New York, 844 pp.

Nixon, P.H., Boyd, F.R., Boullier, A.-M., 1973. The evidence of kimberlite and its inclusions on the constitution of the outer part of the Earth. In: Nixon, P.H. (Ed.), Lesotho Kimberlites. Lesotho National Development, Maseru, pp. 312–318.

Ottolini, L., McDonough, W.F., 1996. Geochemistry of lithium and boron in the mantle: results from studies of peridotites. Journal of Conference Abstracts 1, 446.

Pearson, D.G., 1998. The age of Continental Roots. This volume.

Press, S., Witt, G., Seck, H.A., Ionov, D., Stosch, H.-G., 1986. Spinel peridotite xenoliths from the Tariat depression, Mongolia: I. Major element chemistry and mineralogy of a primitive mantle xenolith suite. Geochimica et Cosmochimica Acta 50, 2587–2599.

Qu, Q., Taylor, L.A., Zhou, X., 1997. Petrology and geochemistry of mantle peridotite xenoliths from SE China. Journal of Petrology 36, 55–79.

Rampone, E., Bottazzi, P., Ottolinin, L., 1991. Complementary Ti and Zr anomalies in orthopyroxene and clinopyroxene from mantle peridotites. Nature 354, 518–520.

Rampone, E., Piccardo, G.B., Vannucci, R., Bottazzi, Ottolini, L., 1993. Subsolidus reactions monitored by trace element partitioning: the spinel- to plagioclase-facies transition in mantle peridotites. Contributions to Mineralogy and Petrology 115, 1–17.

Rudnick, R.L., McDonough, W.F., Orpin, A., 1994. Northern Tanzanian peridotite xenoliths: a comparison with Kaapvaal peridotites and inferences on metasomatic interactions. In: Meyer, H.O.A., Leonardos, O.H. (Eds.), Kimberlites, Related Rocks and Mantle Xenoliths. CPRM Special Publ., Brasilia, pp. 336–353.

Salters, V.J.M., Shimizu, N., 1988. World-wide occurrence of HFSE-depleted mantle. Geochimica et Cosmochimica Acta 52, 2177–2182.

Schmidt, K., Bottazzi, P., Vannucci, R., Mengel, K., 1998. Trace element partitioning between phlogopite, clinopyroxene and leucite lamproite melt. Earth and Planetary Science Letters (in press).

Skewes, M.A., Stern, C.R., 1989. Petrology and geochemistry of alkali basalts and ultramafic inclusions from the Pali–Aike volcanic field in southern Chile and the origin of the Patagonian plateau lavas. Journal of Volcanology and Geothermal Research 6, 3–25.

Stern, C.R., Saul, S., Skewes, M.A., Futa, K., 1989. Garnet peridotite xenoliths from the Pali–Aike alkali basalts of southernmost South America. In: Ross, J.R., et al. (Eds.), Kimberlites and Related Rocks, Vol. 2. Blackwell, Melbourne, pp. 735–744.

Stosch, H.-G., 1982. Rare earth element partitioning between minerals from anhydrous spinel peridotite xenoliths. Geochimica et Cosmochimica Acta 46, 793–811.

Stosch, H.-G., Lugmair, G.W., Kovalenko, V.I., 1986. Spinel peridotite xenoliths from the Tariat depression, Mongolia: II. Geochemistry and Nd and Sr isotopic composition and their implications for the evolution of the subcontinental mantle. Geochimica et Cosmochimica Acta 50, 2601–2614.

Sun, S.-S., McDonough, W.F., 1989. Chemical and isotopic systematics of oceanic basalts: implications for mantle composition and processes. In: Saunders, A.D., Norry, M.J. (Eds.), Magmatism in the Ocean Basins. Geological Society of London, Special Publication 42, 313–345.

Tiepolo, M., Vannucci, R., Zanetti, A., Brumm, R., Foley, S.F., Bottazzi, P., Oberti, R., 1998. Partitioning of Nb and Zr between pargasite/kaersutite and melts in Ti-depleted systems. Mineralogical Magazine 62A, 1519–1520.

Watson, E.B., Harrison, T.M., 1983. Zircon saturation revisited: temperature and composition effects in a variety of crustal magma types. Earth and Planetary Science Letters 64, 295–304.

Watson, E.B., Ben Othman, D., Luck, J.-M., Hofmann, A.W., 1987. Partitioning of U, Pb, Cs, Yb, Hf, Re and Os between chromian diopsidic pyroxene and haplobasaltic liquid. Chemical Geology 62, 191–208.

Webb, S.A., Wood, B.J., 1986. Spinel–pyroxene–garnet relationship and their dependence on Cr/Al ratio. Contributions to Mineralogy and Petrology 92, 471–480.

Zack, T., Foley, S.F., Jenner, G.A., 1997. A consistent partition coefficient set for clinopyroxene, amphibole and garnet from laser ablation microprobe analysis of garnet pyroxenites from Kakanui, New Zealand. Neues Jahrbuch für Mineralogie, Abhandlungen 172, 23–41.

Zinngrebe, E., Foley, S.F., Vannucci, R., Bottazzi, P., Mattey, D.P., 1995. Metasomatism of peridotite by alkaline melt and cognate fluid: microchemical and ion probe evidence from the low-P Inagli Dunite. Extended Abstract 6th International Kimberlite Conference, Novosibirsk, pp. 700–702.

Zorin, Y.A., 1981. The Baikal Rift: an example of the intrusion of asthenospheric material into the lithosphere as the cause of disruption of lithospheric plates. Tectonophysics 73, 91–104.

Zorin, Y.A., Kozhevnikov, V.M., Novoselova, M.R., Turutaov, E.K., 1989. Thickness of the lithosphere beneath the Baikal Rift zone and adjacent regions. Tectonophysics 168, 327–337.